Blind Restoration Algorithm Based on Noise Estimation and Sparse Regularization for Airborne Infrared Image

Yin Xiao, De-Yan Wang, Ya Gao

School of Internet of Things Technology
Wuxi Institute of Technology
Jiangsu Wuxi 214001, China

Shu Yi Guo

2North China University of Water Resources and Electric Power
Zhengzhou 450011, China

ABSTRACT. *Due to many interference factors, airborne infrared camera has a poor imaging quality. The classical image restoration methods can not get better restoration effect for infrared blurry image. In the paper, a blind restoration algorithm of motion blurry images is proposed, which combines noise estimation with sparse regularization. This method effectively utilizes the noise characteristics of infrared imaging camera and the sparse prior information of the edge in infrared image. Firstly, noise distribution in the imaging process is analyzed and the noise is pre-processed. Then, according to the sparse representation theory, sparse prior information of the edges in images is used to guide the restoration of point spread function (PSF). Many simulation experiments show that our proposed algorithm achieves more favorable performance than these existing state-of-the-art algorithms in handing blurry images, which can effectively improve the image quality in the simulation or actual blurred image restoration experiment. In addition, our proposed algorithm also applies to blurred image restoration based on cloud computer,which speeds up restoration speed with online method.*
Keywords: Infrared image; Noise estimation; Sparse regularization; Blind restoration; Point spread function; Prior information.

1. **Introduction.** It is well known that airborne infrared cameras will produce motion blur in the imaging process, which causes image quality is reduced. In other words, the degraded images need to be enhanced and restored. However, since the infrared imaging system is affected by many factors, it is difficult to use a specific point spread function (referred to as PSF) to describe the image degradation process. This is a kind of blind image restoration problem. Due to the lack of prior knowledge of the imaging process, the regularization method is needed to increase the constraint condition. In this paper, an image blind restoration method based on noise analysis and sparse regularization is proposed to improve the image quality. There are many classical algorithms in image restoration, for example, Wiener filtering; RL (Richardson-Lucy) iteration algorithm; least-squares filtering; parameter estimation based blind restoration and so on. These methods have their own advantages and disadvantages, but the most critical problem is that these algorithms are based on some prior knowledge, such as motion blur angle and scale. However, even if the helicopter flight speed, altitude and angle has been known

during the course of the flight, the infrared camera has been in a swing state, it is difficult to determine the specific PSF. In literature [1], a blind restoration algorithm based on motion-blurring parameter estimation is proposed. Firstly, the Cepstrum and Radon transform is used to determine the fuzzy angle. Then, the image is reconstructed by fuzzy scale iteration and Wiener filter. Edge detection is performed in reconstructed image so as to determine the fuzzy scale. The method is simple and effective, but it is only applicable to the blurred image caused by the slow uniform linear motion. It is not suitable for the blurred image caused by the fast-speed motion. Blind restoration algorithm is for solving clear image in which the PSF can be known or unknown, which is a kind of ill-posed problem. Some regularization methods are often used to increase some constraints during the solutions. You et. al [2] proposed an image blind restoration algorithm based on H1 norm normalization method. Chan et al. [3] applied the total variance norm to blind restoration so as to preserve the edge information of the infrared image. Fergus et. al [4] proposed a Bayesian-based blind restoration method for single-motion blurred image.

Krishnan et al [5] proposed a restoration method based on ratio sparse regularization, which can restore various types of degradation image. In literature [6], a multi-regularization optimization method is proposed in the framework of sparse representation theory, which transforms the image restoration problem into a global optimization problem. In literature [7], a blind restoration method combining sparse representation with Weber's law is proposed. In literature[8], the sparse information of natural images is used as a prior knowledge to improve the quality of astronomical observations image in atmospheric turbulence. In literature [9], a natural optical image blind restoration model based on non-convex high-order total variation regularization is proposed for resolving the phenomenon like ringing, trailing and so on in the blind restoration algorithm. In literature [10], a restoration model based on Tikhonov and total variational regularization for mixed constraints is proposed so as to obtain a better restoration effect in the edge region and smooth region of fuzzy image. In the previous study, the most prominent problem is that the restored image will lose some details, which is the sensitivity of the algorithm itself to the noise and the lack of prior information. Since the actual image captured by airborne infrared camera has more serious fuzzy and noise, image noise should be firstly analyzed and processed. Image blind restoration algorithm is an important research direction in the image restoration field, because it is very difficult to reconstruct the concrete degradation process for the blurred image [11-15]. This paper hopes to obtain the clear image directly from the blurred image according to some constraints. Based on the imaging characteristics of helicopter infrared camera, the noise distribution is analyzed firstly and then the point spread function is recovered by sparse prior information, so the target image is obtained by the non-blind restoration algorithm, which is the input image of the next iteration so as to iterate repeatedly to get clear image[16-18]. The rest of our paper is organized as follows: we firstly describe experiment platform and process, especially for sweeping processs of infrared camera in Section 2. In order to effectively utilizes the noise characteristics, nosie distribution is analysed.in Section 3. Our proposed blind restoration based on sparse regularization is detailed in Section 4. In section 5, we present the experiment results and performance analysis against existing state-of-the-art algorithm. The last Section is the conclusion of the whole dissertation

2. **Experimental process.** An infrared camera (wavelength range 7.5 14 m) is mounted on the side of the helicopter along with the sweeping platform and all flight data was recorded using an Inertial Measurement Unit (IMU). Diagram of sweeping platform is shown in Figure 1:
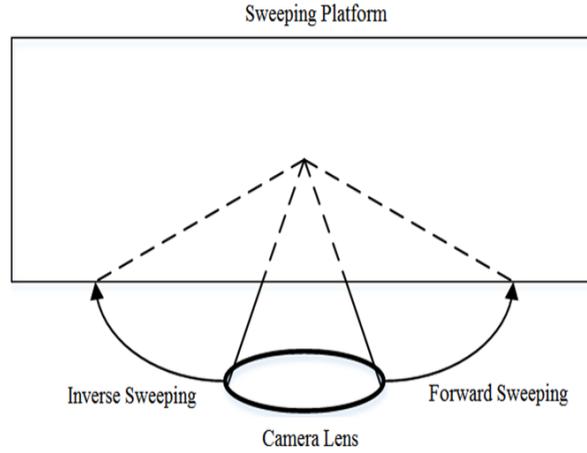
FIGURE 1. Diagram of sweeping platform

The imaging system of our experiment is shown in Fig.2. The focal length of the optical system is f=70mm, the pixel size is $17\mu m$, and the pixel center distance is $17\mu m$. According to the optical system and the size of the detector pixels, the instantaneous field of view angle of the imaging system can be calculated along the scanning direction and the line-column direction, whose expression is shown as follows:

$$\theta = 2\arctan\left(\frac{d}{2(f+d/2)}\right) = 0.014° \tag{1}$$

During the forward flight of the helicopter, the flight height H = 150 m, flight speed v = 90 km/h, long-wave infrared detector exposure time is 10 ms, so the shift number of object scene in the detector plane image is written as follow:

$$N = \frac{vt}{H}\cdot\frac{f}{d} \approx \frac{vt}{H\tan\theta} = \frac{90\text{km/h}\cdot 10\text{ms}}{150\text{m}\cdot\tan(0.014°)} \approx 7 \tag{2}$$

Therefore, the movement angle is the direction of helicopter flight without sweeping whose measured value is north west 15°, and the motion scale is 7 pixels.

2.1. **Imaging data analysis with forward sweeping.** The scanning speed is $W = 18°/s$, and the exposure time of the long-wave infrared detector is t = 10 ms. The shift number of object scene in the detector plane image is written as following formula (3):

$$N = \frac{Wt}{\theta} = \frac{18°/\text{s}\times 10\text{ms}}{0.014°} \approx 13 \tag{3}$$

Thus, the pixel-shift number produced by the forward sweeping can be synthesized as follows:

It can be seen that the movement angle is 28°, and the motion scale is 15 pixels.

2.2. **Imaging data analysis with reverse sweeping.** The scanning speed is W = 60∘/s in reverse sweeping. The shift number of object scene in the detector plane image is written as following formula (4):

$$N = \frac{Wt}{\theta} = \frac{60°/\text{s}\times 10\text{ms}}{0.014°} \approx 43 \tag{4}$$

Thus, the The pixel-shift number produced by the inverse sweeping can be synthesized as follows:

Fig.4 Diagram of inverse sweeping It can be seen that the movement angle is 10°, and the motion scale is 44 pixels.
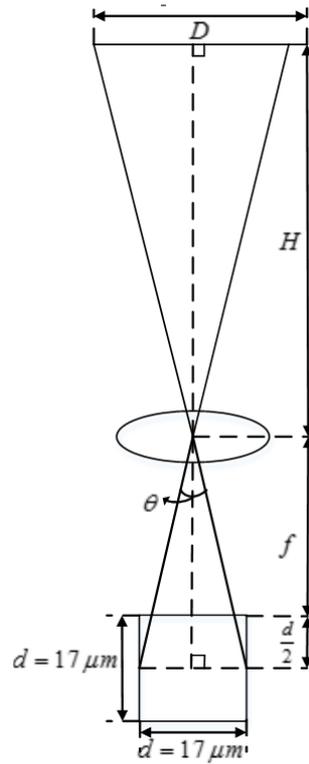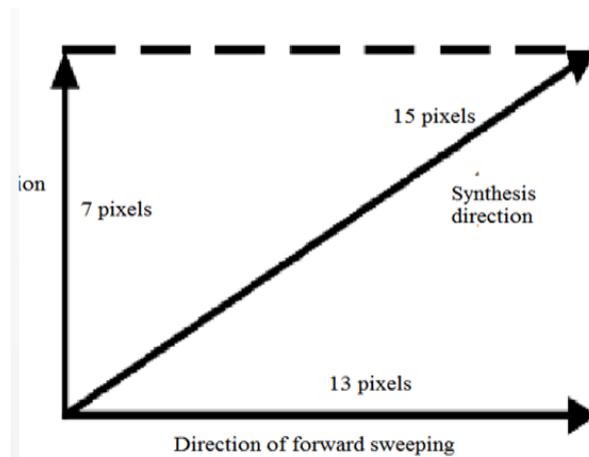
FIGURE 2. Diagram of imaging system

FIGURE 3. Diagram of forward sweeping

3. **Noise analysis.** It is assumed that the pixel displacement caused by the helicopter vibration has the same probability distribution. The attitude angle, angular velocity and acceleration of the helicopter at each moment are obtained by IMU, and the noise caused by the helicopter vibration is tested by the Quantum Quantile Plot so as to show whether the distribution of noise approximates the normal Gaussian distribution. A point coordinate is selected as the reference coordinates when the helicopter hover, it may be set to $O(0,0,0)$. So we can obtain coordinates $O^{'}(X_t, Y_t, Z_t)$ at t time and calculate the distance between $O^{'}$ and O, which can be defined as:

$$\|d\|^2 = (X_t, Y_t, Z_t) \cdot (X_t, Y_t, Z_t)^{\mathrm{T}} \tag{5}$$

(5) Quantum Quantile Plot is adopted to check whether the sample data will be approximately normal distribution. It only need to see whether the points on the Quantum Quantile Plot are close to a straight line, where the detailed algorithm can be referred in literature [11] and [12]. Figure 5 shows sample data of helicopter hover gestures with the standard normal distribution on Quantum Quantile plot. It can be seen that the sample point for the helicopter hover is the coordinate offset quantiles. In other words, the sample points quantile approximately Arrange in a line. Therefore, it is believed that the noise from helicopter vibration approximately obey Gaussian normal distribution with the mean value 3.0815 and the variance 1.9538.
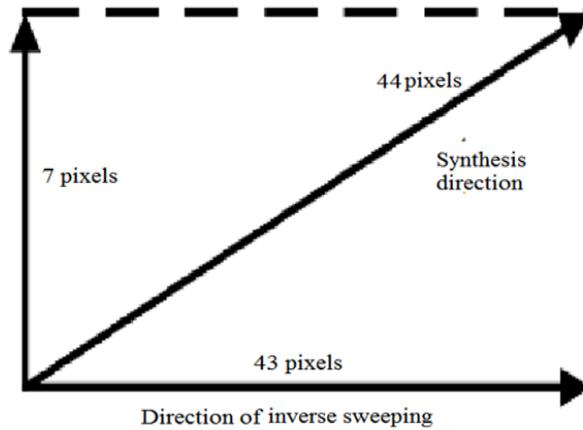

FIGURE 4. Diagram of inverse sweeping

4. **Blind restoration based on sparse regularization.** With the development of image sparse expression theory in recent years, it has been found that the sudden change has a small proportion in infrared images [8], which can guide the image restoration with the sparse prior information of image edge. It is found by Krishnan et al. [5] that the l_1/l_2norm of the image is more suitable for the blind restoration algorithm than thel_1 norm and the $l_2$norm as a constraint, so the l_1/l_2 norm is chosen as the sparse constraint of the image gradient in paper. The degradation model of the image is given by Equation 6:

$$g = f * H + n \qquad (6)$$

where g is the observed blurred image, f is the clear image, H is the point spread function, and n is the noise. According to the analysis in Section 3, we have obtained the noise n approximately obey the Gaussian distribution, so the non-local mean filter is used to pre-process the noise image. In the blind restoration process, the sparse regularization constraint is equivalent to the high-pass filtering of the image. Let us define the regularization operator $\nabla_x = [1, -1]$and$\nabla_y = [1, -1]^{\mathrm{T}}$, and regularization operator is adopted to get high-frequency images$y = [\nabla_x g, \nabla_y g]$. Thus, the fuzzy restoration model is expressed as:

$$\min_{x,k} \lambda \|x * h - y\|_2^2 + \frac{\|x\|_1}{\|x\|_2} + \psi \|h\|_1 \qquad (7)$$

where x is an unknown high-frequency sharpened image, h is an unknown point spread function; $\| \cdot \|_1$ and $\| \cdot \|_2$ is denoted as the norm and l_2 norm, respectively;λ and ψ are the weight parameters,. In this paper, h = 200, = 0.001. Next, x and h are obtained in an iterative manner.

4.1. **Iterative image.** The objective function of the iterative image x can be expressed by Equation 8:

$$\min_x \lambda \|x * h - y\|_2^2 + \frac{\|x\|_1}{\|x\|_2} \tag{8}$$

Since $\|x\|_1/\|x\|_2$ is not convex function, it is difficult to solve the minimum. Therefore, two-layer is adopted to get iterating image, where one-loop iteration for $\|x\|_2$, and the other layer iterates for $\|x\|_1$ on a fixed $\|x\|_2$ basis. In this paper, the number of iteration times for each layer is set to two. After the fixed denominator, the problem can be transformed into solving the convex function minimization problem, which can be written as follows:

$$\min_x \lambda \|Hx - y\|_2^2 + \|x\|_1 \tag{9}$$

Iterative Shrinkage-Thresholding Algorithm (ISTA) is used to solve the objective function (9).

4.2. **The iterative point spread function.** The objective function of the iterative point spread function h can be expressed by Eq. (10)

$$\min_h \lambda \|x * h - y\|_2^2 + \psi\|h\|_1 \tag{10}$$

where h satisfies $h \geq 0 \sum_i h_i = 1$. The objective function (10) can be solved by the Iterative Weighted Least Squares (IWLS)[16-22].

4.3. **Image restoration.** After obtaining the point spread function by iteration, the reconstructed image is obtained by non-blind restoration algorithm. In this paper, the algorithm proposed by Krishnan et al. [5] is used to minimize the estimation error of the point spread function, where the cost function of the algorithm is shown as follows:

$$\min_u \alpha \|u * h - g\|_2^2 + \|\nabla_x g\|_1 + \|\nabla_y g\|_1 \tag{11}$$

where u is the estimated reconstructed image; ∇_x and ∇_y are the regularization operator; is weight, and is set to 200. The resulting image u is used as input to the next iteration, and the above three steps are repeated until the number of iterations is satisfied. The number of iterations is set to 20 in this paper.
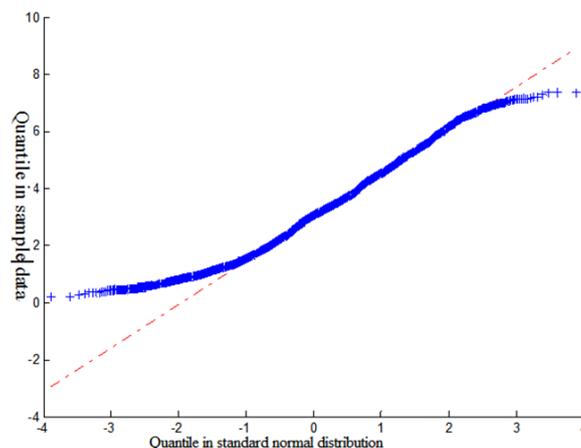

FIGURE 5. Sample data of helicopter hover gestures with the standard normal distribution

5. **Experimental results and analysis.** In this paper, the experiment on the simulation blurred image restoration and the airborne infrared fuzzy image restoration are done respectively. In the simulation experiment, we use the peak signal to noise ratio (PSNR) as the objective quality evaluation method, and the PSNR is calculated as follows:

$$\text{PSNR} = 10 \lg \left(\frac{255^2 \times M \times N}{\sum_{i=1}^{M} \sum_{j=1}^{N} [g(i,j) - \hat{g}(i,j)]^2} \right) \tag{12}$$

where M and N are the length and width of the image, respectively; $g(i,j)$ and $\hat{g}(i,j)$ are the pixel values of the original image and the restoration image at point (i,j) respectively. The larger the PSNR value, the better the image quality. Because there is no clear image as a reference image in the real fuzzy infrared image restoration experiment, this paper uses the gray mean gradient (GMG) as the objective quality evaluation method, GMG calculation method is shown as follows:

$$\text{GMG} = \frac{1}{(M-1)(N-1)} \sum_{i=1}^{M-1} \sum_{j=1}^{N-1} \sqrt{\frac{(\Delta x)^2 + (\Delta y)^2}{2}} \tag{13}$$

where M and N are the length and width of the image, respectively; $\Delta x = g(i+1,j) - g(i,j)$, $\Delta y = g(i,j+1) - g(i,j)$. GMG can better reflect the image contrast and texture characteristics, where the greater value shows the better image quality.

5.1. **Restoration experiment of the simulated blurry image.** Restoration experiment of the simulated blurry image selected the infrared camera to shoot a clear building image. Firstly, motion blur processing is performed on the image with motion angle of 30 and motion scale of 10 pixels, and Gaussian noise is added to the image according to the analysis in Section 3. Figure 6 is a Restoration experiment results of the simulated blurry image. Figure 7 is the point spread function estimated by our proposed algorithm in this paper.
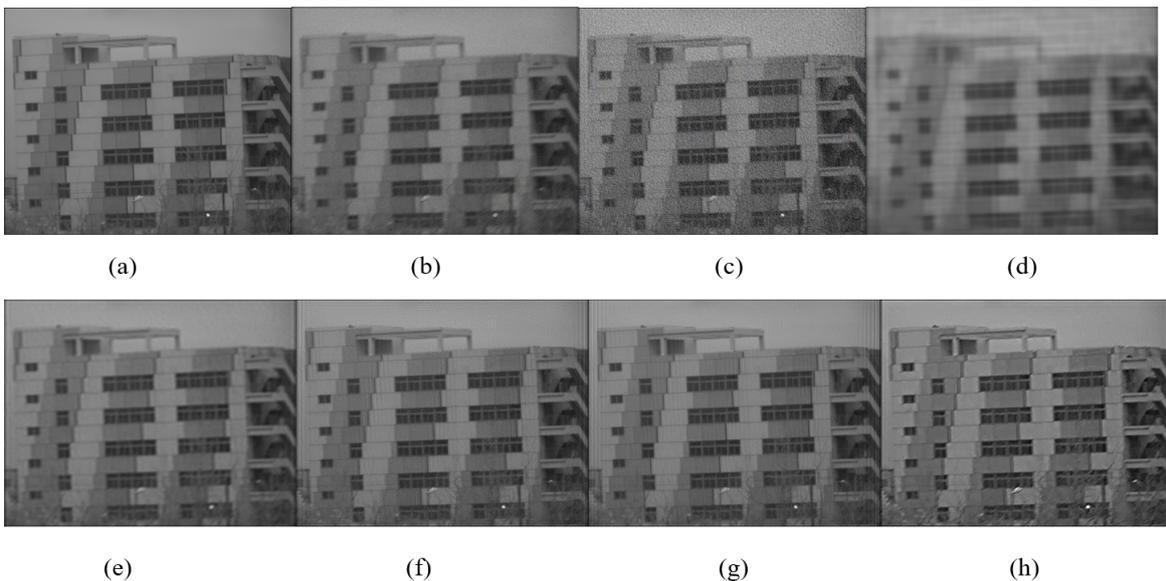

FIGURE 6. (a) original image (b) simulated blurry image (c) Wiener filter (parameter estimation method) (d) Wiener filter (autocorrelation method) (e) constrained least squares method (f) RL method (g) parameter estimation based blind restoration (h) our proposed method

TABLE 1. PSNR and GMG values of each method in simulated blurry image restoration

Image	PSNR(dB)	GMG
Original image	—	3.0182
Simulated blurry image	31.3838	1.6709
Wiener filter (parameter estimation method)	31.8566	3.0030
Wiener filter (autocorrelation method)	25.0889	1.3228
Constrained least squares method	34.3368	1.8954
RL algorithm	37.8597	3.3600
Parameter estimation blind restoration	38.6554	4.2079
Our algorithm	32.2093	3.0243

Table 1 shows the PSNR and GMG of the infrared simulated blurry image in the blurred image restoration experiment. The GMG value is calculated in the simulation experiment so as to make a reference to the real fuzzy image restoration experiment. The number of RL iterations is 15 times.
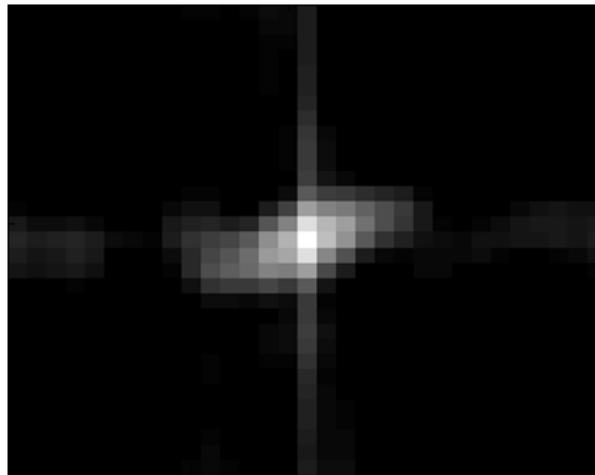

FIGURE 7. PSF estimation of the simulated blurry image

It can be seen from the PSNR value that all algorithms (except Wiener filter with auto-correlation method) can get better quality images. But the better image quality can not represent the image contour more clearly. For example, the PSNR of the constrained least squares method is larger than that of the simulated blurry image, but the GMG value is smaller than that of the original image, which shows that the result of this method is not too different from the original image, but the image detail is not enhanced. The GMG value of the restored image obtained by our proposed algorithm is close with the original image, indicating that most of the details have been restored. GMG value of the RL iteration and the parameter estimation blind restoration algorithm is more than the original image, indicating that the restoration image may also exist ringing phenomenon.

5.2. **Real blurry image restoration experiment.** In the first section of the paper, we have estimated the motion blurring angle and scale of the infrared image in the three cases of no-sweeping, forward sweeping and reverse sweeping. According to the estimation
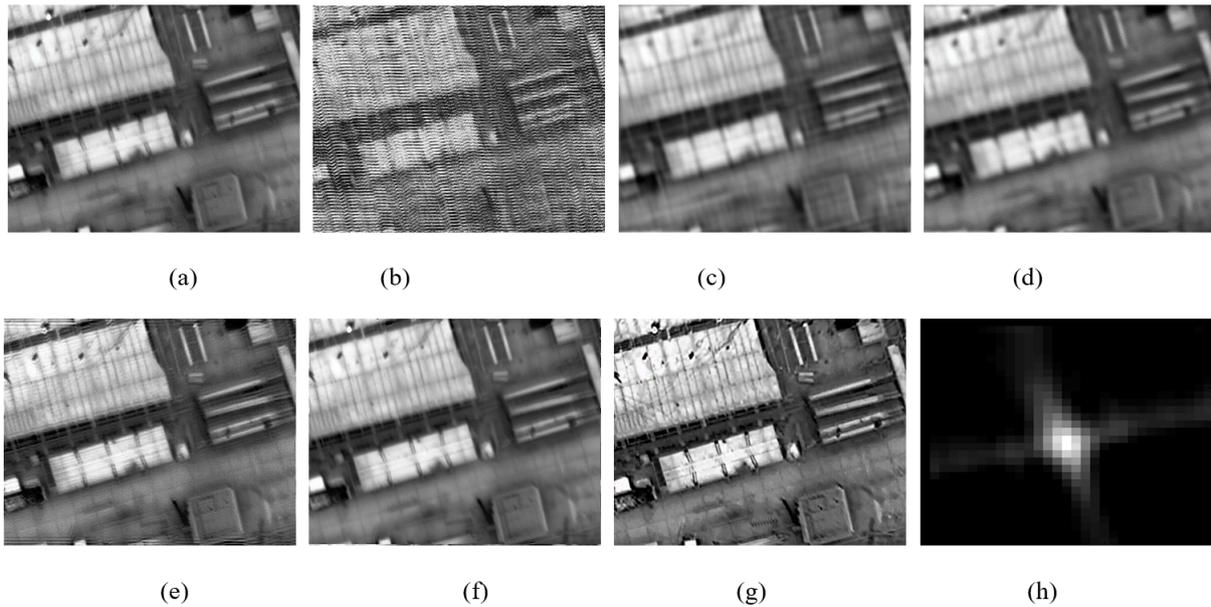
FIGURE 8. (a) real blurry image without sweeping (b) Wiener filter (parameter estimation method) (c) Wiener filter (autocorrelation method) (d) constrained least squares method (e) RL method (f) parameter estimation blind restoration (g) our method (h) PSF

result, the fuzzy image is reconstructed by Wiener filtering, constrained least squares filtering and so on. In this paper, the PSF is obtained by sparse prior information, and the blurred image is restored according to the PSF. Figure 8 shows the results of the blur image restoration without sweeping. Figure 9 is the result of the motion blurred image restoration with forward sweeping. Fig. 10 shows the results of the blurring image restoration with inverse sweeping
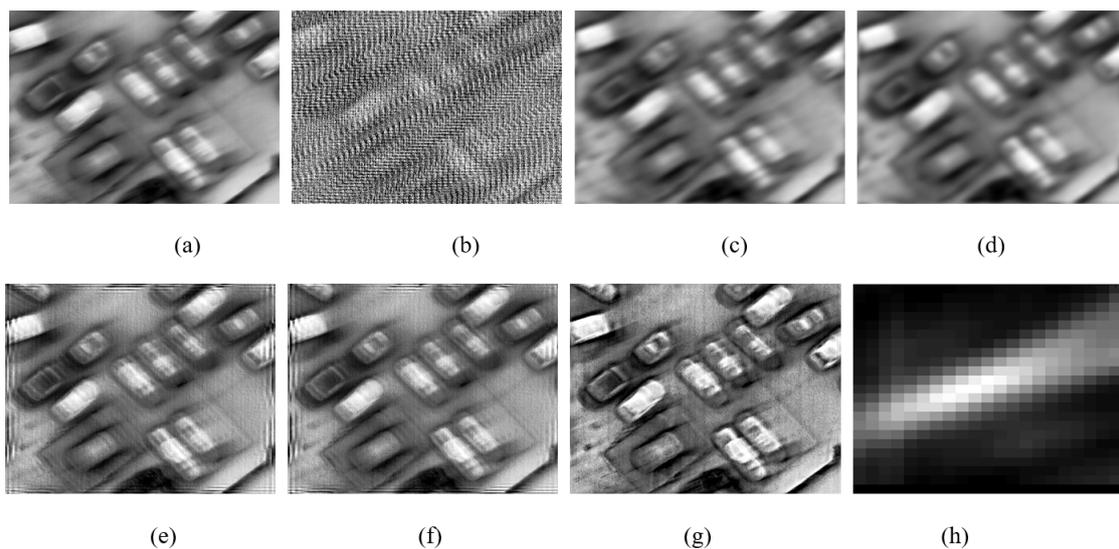

FIGURE 9. (a) real blurry image with forward sweeping (b) Wiener filter (parameter estimation method) (c) Wiener filter (autocorrelation method) (d) constrained least squares method (e) RL method (f) parameter estimation blind restoration (g) our method (h) PSF

TABLE 2. GMG values of each method in real blurry image restoration

| Image	No-sweeping	Forward sweeping	Inverse sweeping
Real blurry image	3.7287	4.2525	3.2803
Wiener filter (parameter estimation method)	-	-	-
Wiener filter (autocorrelation method)	2.3776	1.9974	1.2607
Constrained least squares method	2.2092	1.8931	1.2102
RL algorithm	5.0247	11.9162	7.7168
Parameter estimation blind restoration	3.5638	12.1135	—
Our algorithm	5.7638	12.3131	8.1325
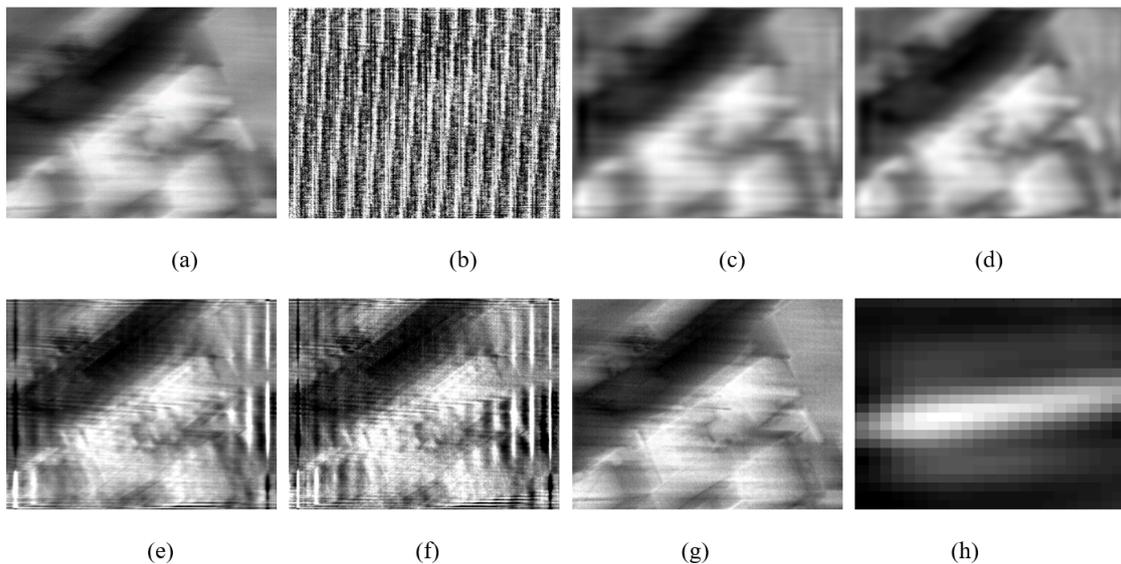
FIGURE 10. (a) real blurry image with inverse sweeping (b) Wiener filter (parameter estimation method) (c) Wiener filter (autocorrelation method) (d) constrained least squares method (e) RL method (f) parameter estimation blind restoration (g) our method (h) PSF

Table 2 shows the GMG values of the restoration results in the real blurry image. According to Eq. 13, the larger the GMG is, the better the image quality. In Table 2, "-" indicates that the target in the restored image can not be identified, and it is not meaningful to calculate the restored image GMG. The number of RL iterations is 15 times. According to the experimental results, we can see that our proposed method can improve the quality of the image, especially in the case of a lack of prior conditions; It is not difficult to find from the PSNR value and the GMG value that the other algorithms depend on the fuzzy angle and the fuzzy scale estimation. The slight error will affect the image restoration effect, while the PSF in our algorithm is recovered by the sparse prior information, which can effectively improve the image quality

6. **Conclusions.** The motion blurred image restoration problem of helicopter infrared camera is an ill-posed problem. Due to the lack of prior knowledge of the imaging process, classical image restoration methods are limited in image processing. In this paper, we propose a blind restoration algorithm of motion blurry images, which combines noise analysis with sparse regularization. This method effectively utilizes the noise characteristics of infrared camera imaging and the sparse prior information that the edge of infrared image obeys. The experimental results show that the method proposed in paper can effectively improve the image quality in the simulation or actual blurred image restoration experiment. Compared with various existing state-of-the-art image restoration algorithms, our proposed algorithm has a good stability and high robustness in the process of restoration. In addition, our proposed algorithm also applies to blurred image restoration based on cloud computer,which speeds up restoration speed with online method.

REFERENCES

[1] B. Bai, J. Yi, Parameter estimation method of infrared motion blur image *Journal of Transducer and Microsystem,*, vol. 34, no. 9, pp. 27-29. 2015

[2] Y. -L. You, M. Kaveh. A Regularization Approach to Joint Blur Identification and Image Restoration , *Journal of IEEE Transactions on Image Processing,* vol. 5 , no. 3, pp. 416-428, 1996.

[3] T. F. Chan, C.-K. Wong, Total Variation Blind Deconvolution, *Journal of IEEE Transactions on Image Processing*, vol. 7 , no. 3, pp. 370-375, 1998.

[4] R. Fergus, B. Singh, A. Hertzmann et al. Removing Camera Shake from a Single Photograph , *Journal of ACM Transactions on Graphics*, vol. 25 , no. 3, pp. 787-794, 2010.

[5] D. Krishnan, T. Tay, Rob Fergus. Blind Deconvolution Using a Normalized Sparsity Measure, *Journal of IEEE Computer Vision and Pattern Recognition*, vol. 42 , no. 7, pp. 233-240, 2011.

[6] S. Xiao, Y. Zheng, Multi-regularized image restoration based on sparse representation , *Journal of Computer Engineering and Applications*, vol. 51 , no. 12, pp. 203-207, 2015.

[7] C. Y. Liu, F. Chang, Blind restoring of moving images based on sparse representation and Weber's law, *Journal of , Editorial Office of Optics and Precision Engineeri,* vol.23 , no. 2, pp. 600-608, 2015.2.

[8] L. Hui, Q. Linhong, N. Yang, et al .. Blind restoration of turbulence images based on edge detection and sparse constraints , *Journal of , Journal of Instrumentation,* 2015.4,36 , no. 4, pp. 721-728.

[9] C. -Z. Guo, Z. Y. Qin , Blind restoration of non-convex high order total variation normalized natural optical images, *Journal of , Optics and Precision Engineering,* vol.23 , no. 12, pp. 3490-3499, 2015.12.

[10] J. B. Li, R. Ma, D. Y. Li, et al. Blinded-Blurring Method Based on Tikhonov and Total Variation Regularization Mixed Constraints, *Journal of , Journal of Nanjing University of Posts and Telecommunications,* vol.36 , no. 3, pp. 68-73, 2016.

[11] K. Bahrami, A. C. Kot, and J. Fan, A novel approach for partial blur detection and segmentation,*in Proc. IEEE Int. Conf. Image Process. ,* 2013, pp. 1-6.

[12] C. Tang, C. Hou, and Z. Song, Defocus map estimation from a single image via spectrum contrast,*Opt. Lett.,* vol. 38, no. 10, pp. 1706-1708, 2013.

[13] Z. H. Tang, S. Z. Wang et al. Bayesian Framework with Non-local and Low-rank Constraint for Image Reconstruction, in *Journal of Physics: Conference Series, CCISP2017.* 787, no. 1). doi: 10.1088/ 1742-6596/ 787/1/012008.

[14] P. Birch, A. Buchanan, R. Young, and C. Chatwin, Depth from structured defocus that is independent of the object reectivity function,*Opt. lett.,* vol. 36, no. 12, pp. 2194-2196, 2011.

[15] X. Yu, X. Zhao, Y. Sui, and L. Zhang, Handling noise in single image defocus map estimation by using directional lters,*Opt. lett.,* vol. 39, no. 21, pp. 6281-6284, 2014.

[16] J. Lin, X. Ji, W. Xu, and Q. Dai, Absolute depth estimation from a single defocused image,*IEEE Trans. Image Process.,* vol. 22, no. 11, pp. 4545-4550, Nov. 2013.

[17] S.-O. Shim and T.-S. Choi, Depth from focus based on combinatorial optimization, *Opt. lett.,* vol. 35, no. 12, pp. 1956-1958, 2010.

[18] F. Diaz, F. Goudail, B. Loiseaux, and J.-P. Huignard, Increase in depth of eld taking into account deconvolution by optimization of pupil mask, *Opt. lett.,* vol. 34, no. 19, pp. 2970-2972, 2009.

[19] L. DAndres, J. Salvador, A. Kochale, and S. Susstrunk, Non-parametric blur map regression for depth of eld extension, *IEEE Trans. Image Process.,* vol. 25, no. 4, pp. 1660-1673, Apr. 2016.

[20] P. Jiang, H. Ling, J. Yu, and J. Peng, Salient region detection by ufo: Uniqueness, focusness and objectness, *in Proc. IEEE Int. Conf. Comput. Vis*, pp. 1976-1983, 2013.

[21] S. H. Chen, S. Y. Ko, and S. Chen, Robust Music Genre Classification Based on Sparse tation and Wavelet Packet Transform with Discrete Trigonometric Transform, *Journal of Network Intelligence,* vol. 1, no. 2, pp. 67-81, May 2016.

[22] Qi. X. Feng, X. Zhu and J. S. Pan, Novel Classification Rule of Two-Phase Test Sample Sparse Representation, *OPTIK-International Journal for Light and Electron Optics,* vol. 125, no. 19, pp. 5825-5832, 2014.